THE RADIAL EVOLUTION OF THE SOLAR WIND, 1-10 AU

P. R. Gazis and A. J. Lazarus
Center for Space Research and Department of Physics,
Massachusetts Institute of Technology
Cambridge, MA 02139

ABSTRACT

We review the interplanetary plasma and magnetic field observations from 1 to 10 AU. Over this distance 1) no clear reduction in average speed is seen, the range of wind speeds becomes smaller though high speed streams are still observed; 2) the density, temperature and magnetic field profiles become dominated by the large values seen in the "co-rotating interaction regions"; 3) the temperature falls more slowly than would be expected from a simple, adiabatic model; 4) co-rotating shocks appear beyond ~3 AU in Voyager data as opposed to beyond ~1.5 AU in the Pioneer data; 5) reverse shocks appear later than forward shocks: reverse shocks do not begin to appear until ~4 AU; 6) reverse shocks appear to decay more rapidly than forward shocks. No clear effect due to interaction with the interstellar medium has been seen in this radial range.

Solar Wind Bulk Parameters

In this paper we shall discuss observations of the the solar wind between 1 and 10 AU. The data were taken by the plasma science experiment aboard the Voyager 1 and 2 spacecraft between day 260 of 1977 and day 200 of 1980. Data taken by the MIT IMP plasma experiment aboard the IMP 8 spacecraft at 1 AU during the same time period were used to enable us to distinguish between radial and temporal variations in the solar wind.

Figure 1 shows solar wind bulk parameters observed by Voyager 1 at 1.3 and at 5.8 AU. One-hour averages of proton bulk velocity, number density, and temperature are plotted against time for two solar rotations. The density has been multiplied by heliocentric distance squared to account for an assumed radial expansion.

The velocity trace at 1.3 AU shows the characteristic pattern of high and low speed streams in the solar wind. Four high speed streams are observed in this time period, or two streams per solar rotation. The velocity varies smoothly; there are no signs of co-rotating shocks. (The apparent velocity jump on day 287 does not have a correlated density or temperature jump and is not a shock. There may be a shock on day 300, but it does not recur in the next solar rotation and thus is not a long-term stream-associated event.) At this heliocentric distance, the velocity and density are almost anticorrelated, as if the solar wind mass flux were remaining constant in time. This type of behavior has been observed from the Helios spacecraft at a smaller heliocentric distance. There is also a correlation between velocity and temperature. These correlations will be discussed at greater length later.
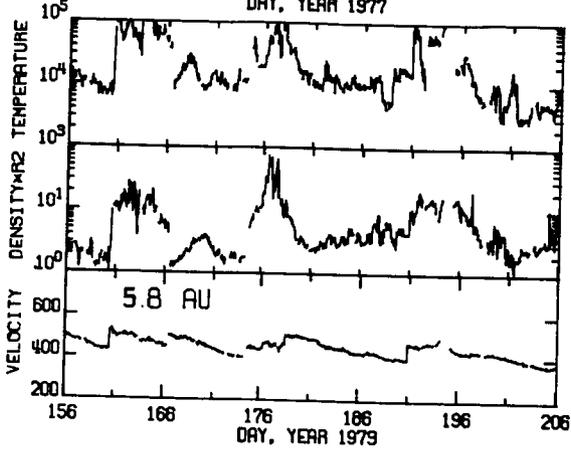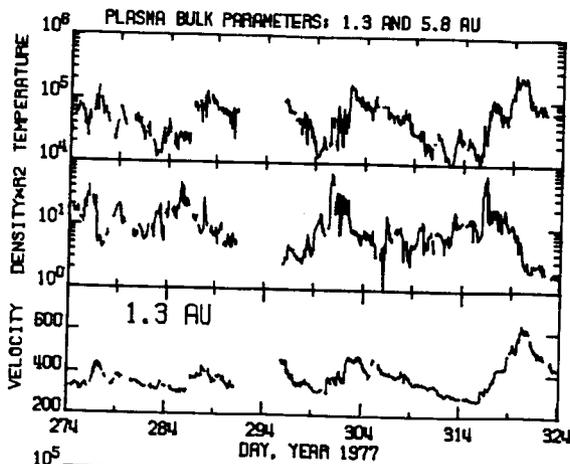
Figure 1: One-hour averages of the solar wind bulk velocity, density, and proton temperature observed from Voyager 1 are plotted against time for two solar rotations at 1.3 AU and at 5.8 AU. The density has been multiplied by heliocentric distance squared to account for an assumed radial expansion.
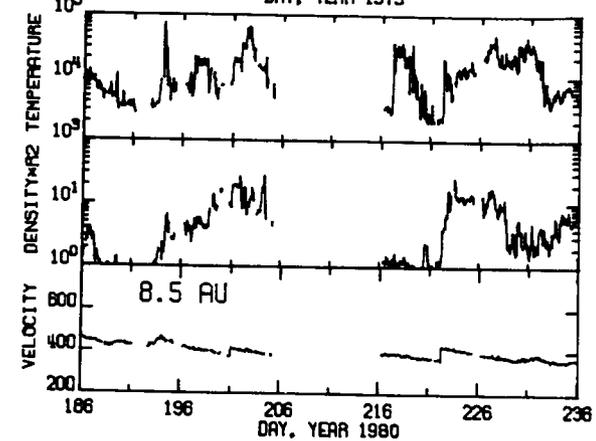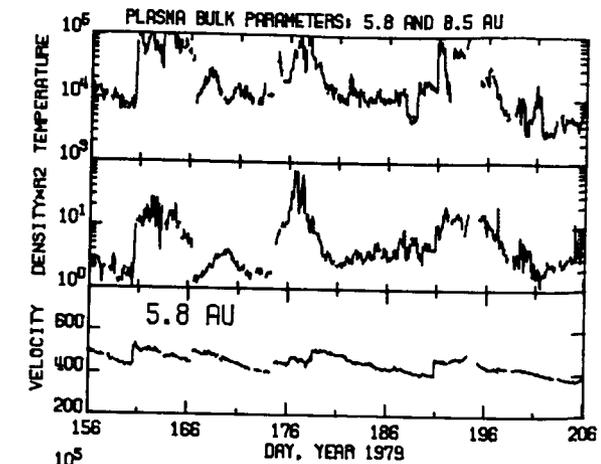
Figure 2: The solar wind bulk velocity, density, and proton temperature plotted against time for two solar rotations at 5.8 AU and at 8.5 AU. Again, the density has been multiplied by the square of heliocentric distance. The top three panels are identical with the bottom three panels of Figure 1.

At 5.8 AU, the character of the solar wind has changed markedly. As at 1.3 AU, two high speed streams are observed per solar rotation, but the smoothly varying velocity profile that was observed at 1.3 AU has been replaced by a new pattern of interaction regions bounded by shocks as was observed by the Pioneer spacecraft [Smith and Wolfe, 1976]. The shocks are observed on days 161, 167, 174, 179, and 191. The interaction regions run from day 161 to day 167, from day 174 to day 179, and from day 191 to approximately day 199. The density and temperature are high in the interaction regions and low in the surrounding streams.

Figure 2 shows a comparison of the solar wind data taken at 5.8 AU with data taken by Voyager 1 at 8.5 AU. The top three panels are identical with the bottom panels of Figure 1.

510

At 8.5 AU, from day 216 onwards, one can see the same structure of streams separated by interaction regions as was seen at 5.8 AU. A shock on day 252, preceeds an interaction region extending from day 252 to approximatly day 263. But while the density and temperature still vary over a factor of ten or more, the range of the velocity variations observed at 8.3 AU is much reduced compared with that observed at 5.8 AU, which in turn is smaller than that observed at 1.3 AU. Furthermore, the stream structure is not always well defined. In the first half of the time period shown in the figure (from day 186 to day 206) it is possible to observe a correlated density and temperature enhancement, but the velocity structure is indistinct and it is difficult to locate the shocks. The prominence of regions of enhanced temperature and density, and hence of enhanced total pressure, is characteristic of the solar wind at these large heliocentric distances.

The first two figures showed the details of the variation of solar wind bulk parameters during a solar rotation. It is interesting to look at the variation of average solar wind parameters with heliocentric radius. Many comparisons have been made of solar wind data observed at different spacecraft at different heliocentric radii during the limited time periods surrounding spacecraft lineups [Collard and Wolfe, 1974; Smith and Wolfe, 1979; Burlaga et al, 1980; Collard et al, 1982]. One can compare data taken at different spacecraft over longer time periods by taking into account the solar wind travel time and the longitudinal separation between the two spacecraft [Gazis and Lazarus, 1982; Burlaga et al, 1983]. A better way to observe large scale radial trends in solar wind parameters is to compare solar rotation averages of solar wind data taken by two spacecraft at different heliocentric radii.

Figure 3 shows a plot of the averages of the solar wind bulk velocity, density, and proton temperature versus heliocentric radius. Each average was taken over two solar rotations. The filled symbols represent data taken by Voyager 1: the open symbols represent data taken by the IMP spacecraft over a corresponding time period, allowing for the effects of solar wind travel time and the longitudinal separation between the two spacecraft. The vertical bars represent the width of the distribution of one-hour averages of each parameter during the averaging period.

Between 1 and 10 AU, the solar wind velocity is seen to remain fairly constant. While there are minor short term fluctuations, the average velocity measured at Voyager and the average velocity measured at IMP change together, indicating that the changes are temporal rather than radial variations. The discrepancy between the average velocity seen by Voyager at 6 AU and the velocity seen at IMP over the corresponding time period is due to a large flare that was seen at Voyager near day 260 of 1979 but was not seen at IMP. This event shows up elsewhere in our data. There is certainly no sign of any long term radial acceleration or deceleration of the solar wind.

The density, N, has been multiplied by the heliocentric radius squared to account for an assumed radial expansion. The resultant quantity NR^2 remains fairly constant with heliocentric radius. There are small variations in the density seen both at Voyager and at IMP which are evidentally temporal effects. The long term decrease in density seen at Voyager is also observed
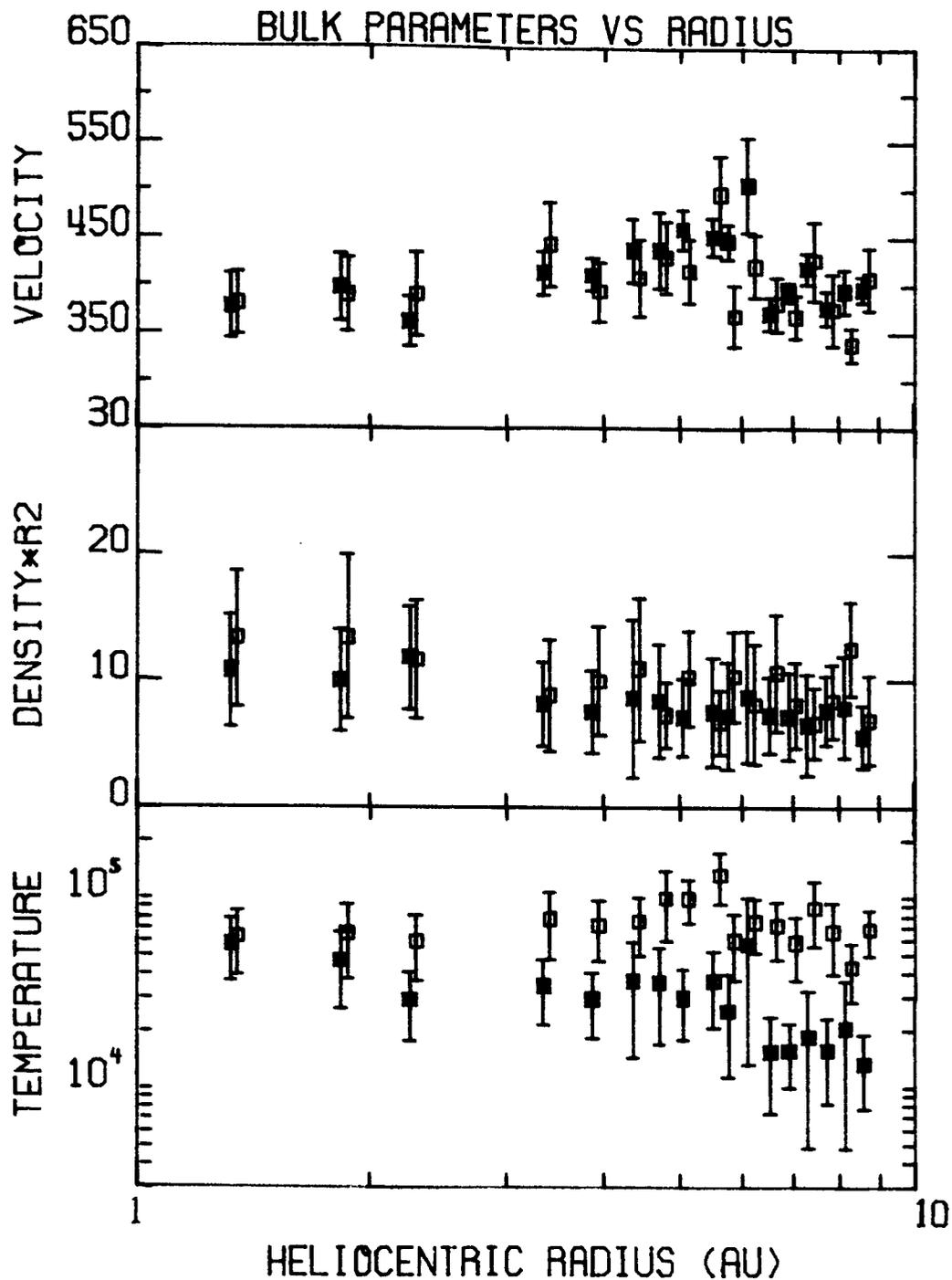
Figure 3: Two-solar-rotation averages of the solar wind bulk velocity, density, and proton temperature are plotted versus heliocentric distance. The filled symbols represent data taken by Voyager 1, the open symbols represent data taken by the IMP spacecraft over a corresponding time period, allowing for the effects of solar wind travel time and the longitudinal separation between the two spacecraft. The vertical bars represent the width of the distribution of one-hour averages of each parameter during the averaging period.

at 1 AU by the IMP spacecraft for this time period (1977 to late 1980). This decrease was also seen by the Helios spacecraft (Schwenn, 1982).

The solar wind proton temperature decreases with increasing heliocentric radius relatively slowly, approximately as $R^{-2/3}$. The temperature at 10 AU is thus a factor of ten higher than would be predicted from the temperature at 1 AU, assuming that the solar wind expanded adiabatically as a perfect gas with $\gamma=5/3$. This type of radial profile has also been observed in data taken by the Pioneer spacecraft [Smith and Wolfe, 1979; Kaiser, 1983]. The temperature decreases more or less monotonically with increasing heliocentric radius. There is no sign of any minimum, such as has been suggested might be the case due to an interaction with the interstellar medium [Holzer, 1972; Axford, 1973; Holzer, 1977]. It has been suggested by Goldstein and Jokipii [1977] that heating of the solar wind due to the interaction between high and low speed streams will produce a local minimum in solar wind temperature between 2 and 3 AU. However, the existence of such a well-defined local minimum is dependent upon the assumption that the solar wind velocity structure is very regular, which was not the case from late 1977 to late 1980.

Figure 4 is a two-dimensional contour plot showing the correlation of density versus bulk velocity. Each contour is at 50% the level of the preceeding one. The density has been multiplied by the heliocentric radius squared to account for an assumed radial expansion. Each panel is constructed from hourly averages of Voyager 1 data over two solar rotations.

The top panel of Figure 4 shows the correlation at 1.3 AU. At this heliocentric distance, the velocity appears to be anti-correlated with density. This anti-correlation is particularly evident if one examines the lower left hand boundaries of the contours.

Goldstein and Jokipii [1977] suggested that this anti-correlation between velocity and density at 1 AU would disappear at larger heliocentric radii due to the interaction between high and low speed streams in the solar wind. The second panel of Figure 4 shows the correlation at 5.8 AU. Here the range of observed velocities is much less than that observed at 1.3 AU. The anti-correlation of density and velocity observed at 1.3 AU has disappeared. Note, however, the new peak in the contours at $V\cong450$ km-sec^{-1}, and $NR^2\cong15$ cm^{-3}, which corresponds to the material at high density and intermediate velocity which has collected in the interaction regions.

The last panel of Figure 4 shows the correlation at 8.5 AU. One sees a more pronounced version of the picture seen at 5.8 AU: The velocity range is smaller still, there is no sign of an anti-correlation between density and velocity, and the peak of material at intermediate velocity and high density in the interaction regions has become clearer.

The three panels of Figure 5 show plots of the correlation between velocity and thermal speed at 1.3, 5.8 and 8.5 AU. At 1.3 AU, as shown in the top panel, the correlation between velocity and thermal speed is quite dramatic. The solar wind at 1.3 AU is seen to be maintaining a flow with an almost constant thermal Mach number, $M_t\cong8$.
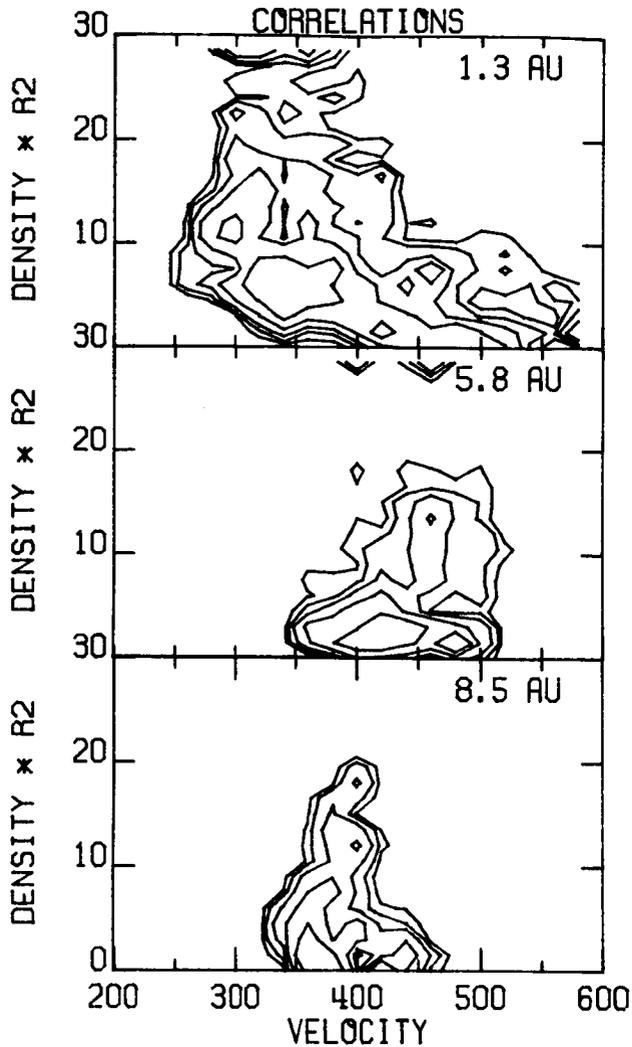
Figure 4: Two-dimensional contour plots showing the correlation of density versus bulk velocity at 1.3, 5.8 and 8.5 AU. Each panel is a plot of hourly averages of Voyager 1 data over two solar rotations. The density has been multiplied by the heliocentric radius squared to account for an assumed radial expansion.
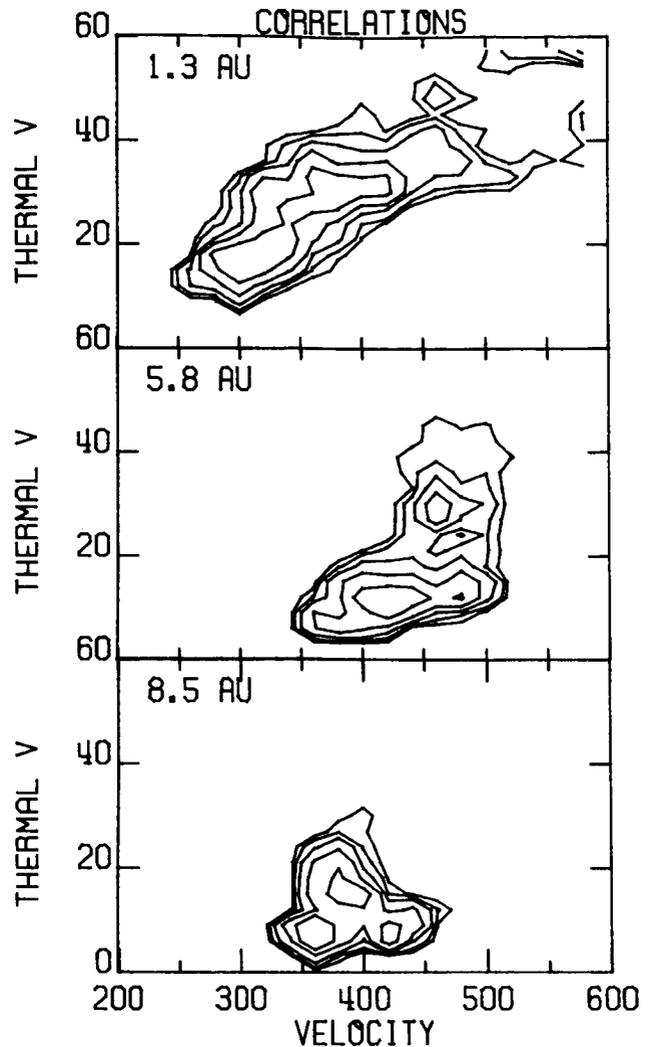
Figure 5: Two-dimensional contour plots showing the correlation of thermal speed versus bulk velocity at 1.3, 5.8 and 8.5 AU. Each panel is a plot of hourly averages of Voyager 1 data over two solar rotations.

Since the solar wind is observed to cool with increasing heliocentric radius, one might expect the thermal Mach number of the solar wind to increase with increasing heliocentric radius. As can be seen in the second panel (5.8 AU), this increase in thermal Mach number does indeed occur. In addition, a new peak has formed in the contours at an intermediate velocity $V \cong 450$ km-s^{-1}, and most probable thermal speed $W \cong 30$ km-s^{-1}. As in the last two panels of Figure 4, this new peak is due to material which has accumulated in the interaction regions.

At 8.5 AU, the thermal Mach number of the flow has increased still further, and the peak due to material in the interaction regions has become still stronger.

In summary, the average solar wind bulk velocity remains constant between 1 and 10 AU; there is no sign of any long term acceleration or deceleration of the solar wind. The average density of the solar wind varies as R^{-2}, which is consistent with uniform radial expansion; there is no sign of any lattitudinal divergence or convergence of the solar wind flow. The average proton temperature varies as $R^{-2/3}$, slower than would be expected for any adiabatic law. The radial profile of the average proton temperature shows no sign of any effect due to the interaction of the solar wind with the interstellar medium.

Co-rotating Shocks in the Solar Wind

One of the more prominent physical effects in the solar wind at large heliocentric radii is the appearance of co-rotating shocks. We made a survey of all shocks seen by the Voyager 1 spacecraft between day 260 of 1977 and day 200 of 1980. It was difficult to detect shocks with velocity jumps less than 20 km-s^{-1} reliably from our high resolution plasma data. However since the shock velocity proved to be generally of the order of twice the velocity jump, and since the observed Alfven speeds were almost always greater than 40 km-s^{-1}, we feel confident that we have observed most of the _fast_ shocks in the solar wind. Nevertheless, this lower threshold of approximately 20 km-s^{-1} must be kept in mind when examining the data which follow.

Numerous theoretical models have been made of the solar wind stream structure and the onset and structure of co-rotating shocks in the solar wind [Hundhausen, 1973; Gosling et al, 1976; Siscoe, 1977; Pizzo, 1982]. The predicted location of shock formation generally lies between 1 and 3 AU and it is predicted that reverse shocks will form before the forward shocks.

Figure 6 shows a plot of the frequency of occurence of forward and reverse fast shocks plotted versus heliocentric radius. (At the Solar Wind V conference we showed plots of shock frequency and average parameters for all shocks. Here we show plots of data for fast shocks only) The frequency is a running average obtained from groups of twelve successive shocks. In the period during which our observations were made, the forward shocks were first observed in the region beyond 3 AU. The exact heliocentric radius at which the forward shocks began to form cannot be determined more precisely from the Voyager 1 data because the Voyager 1 plasma experiment was not operational between 2 and 3 AU. The reverse shocks form later than the forward shocks: Reverse shocks did not begin to appear in our data until the spacecraft had reached a heliocentric distance of 4 AU. The reverse shocks were only half as numerous as the forward shocks. Furthermore, the reverse shocks appear to "disappear" sooner than the forward shocks as they propagate outward from the sun, though this may be a consequence of our detection threshold of approximately 20 km-s^{-1}.

It is interesting to observe the radial variation of various parameters related to shock strength: Figure 7 shows a plot of the radial variation of the average of the density ratio for forward and reverse fast shocks. The
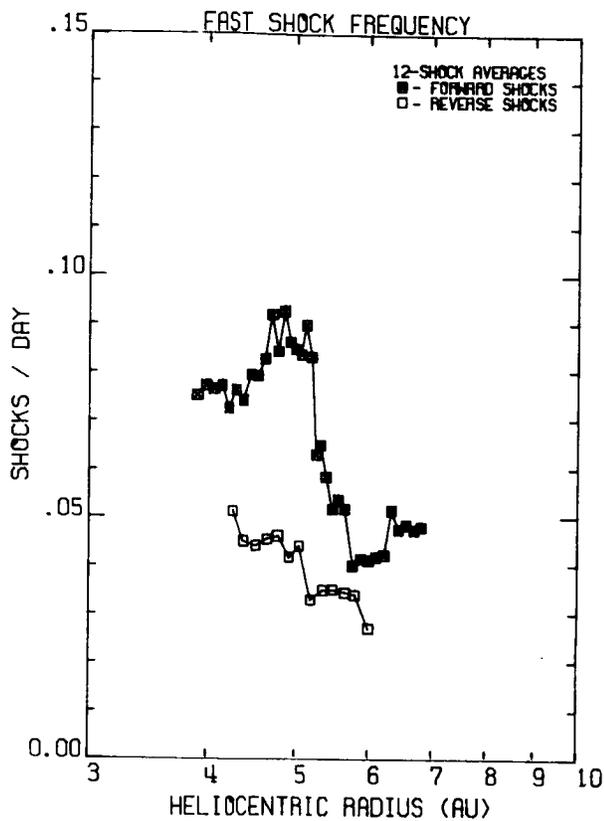
Figure 6: The frequency of occurence of forward and reverse fast shocks plotted versus heliocentric radius. The frequency is a running average over groups of twelve successive shocks. The filled symbols represent averages over forward shocks, the open symbols represent averages over reverse shocks. Note the one event per solar rotation is ∼0.37 events per day.
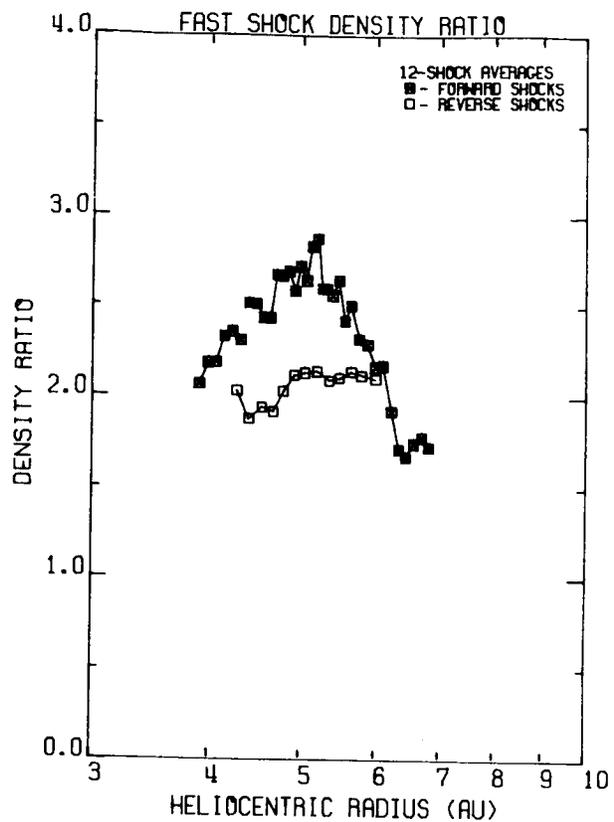
Figure 7: The radial variation of the average of the density ratio for forward and reverse fast shocks. The density has been averaged over groups of twelve successive shocks. The filled symbols represent averages over forward shocks, the open symbols represent averages over reverse shocks.

density ratio has been averaged over groups of twelve successive shocks. The average density ratio of the forward shocks does not appear to vary strongly with heliocentric distance. While the density ratio across individual shocks was observed to vary between 1 and the theoretical maximum of 4, the twelve-shock-average density ratio only varies between 1.7 and 3. The average density ratio of the reverse shocks also does not appear to depend upon heliocentric distance. The reverse shocks are weaker on the average than the forward shocks. While the density ratio across individual reverse shocks also was observed to vary between 1 and 4, the average density ratio across the reverse shocks remains in the vicinity of 2.

Figure 8 shows a plot versus heliocentric distance of twelve-shock running averages of the velocity jump across forward and reverse fast shocks. As in Figure 7, the forward shocks are once more seen to be stronger than the reverse shocks. The velocity jump across the forward shocks is larger, and
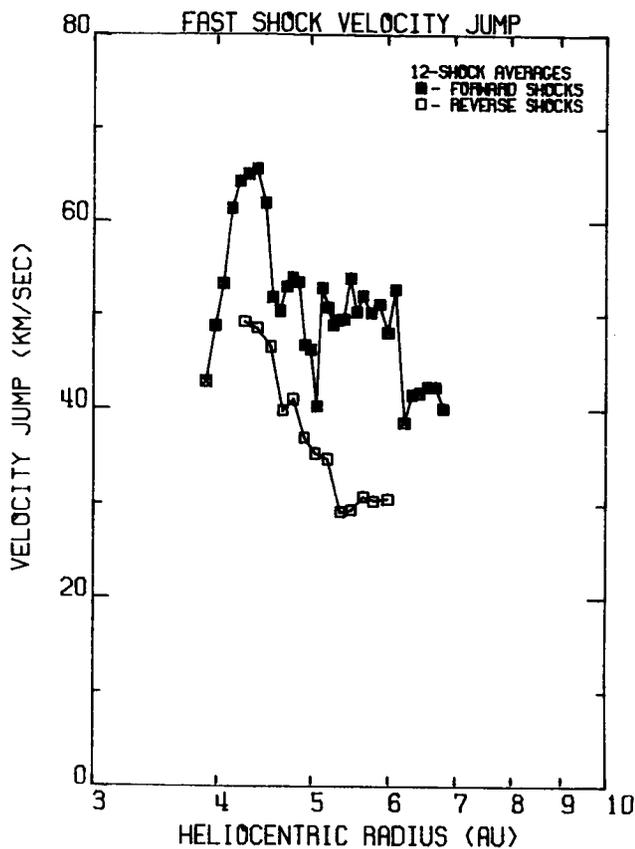
Figure 8: The radial variation of the average of the velocity jump across the shocks for forward shocks and reverse fast shocks. The shock velocity jump has been averaged over groups of twelve successive shocks. The filled symbols represent averages over forward shocks, the open symbols represent averages over reverse shocks.
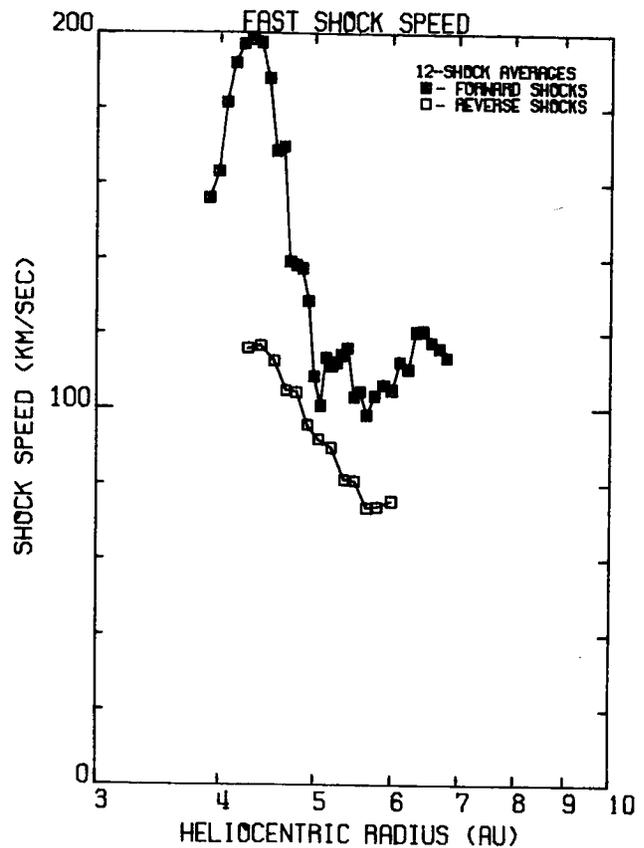
Figure 9: The radial variation of the average of the shock speed for forward shocks and reverse fast shocks. The shock speed is measured relative to the unshocked medium. The shock speed has been averaged over groups of twelve successive shocks. The filled symbols represent averages over forward shocks, the empty symbols represent averages over reverse shocks.

decreases more slowly with increasing distance than does the velocity jump across the reverse shocks.

Since we measure the vector velocities and magnetic fields before and after each shock, there are a number of means by which we can attempt to determine the shock speeds. Figure 9 shows a plot of the twelve shock running average of the shock speeds for forward and reverse fast shocks plotted versus heliocentric distance. In view of the previous results, it is not surprising to note that the forward shocks are faster and remain faster longer than the reverse shocks.

Figure 10 shows a schematic representation of the velocity profile across an interaction region. The top panel shows the velocity profile of an

Schematic Representation of an Interaction Region

Interaction Region

Forward Shock   Reverse Shock

V   t = 0 ΔV_i $\Delta V_2 \delta t$

$\Delta V_i \delta t$ ΔV_i to Sun

V   t = δt $\Delta V_2' < \Delta V_2$ $\Delta V_i' < \Delta V_i$ to Sun
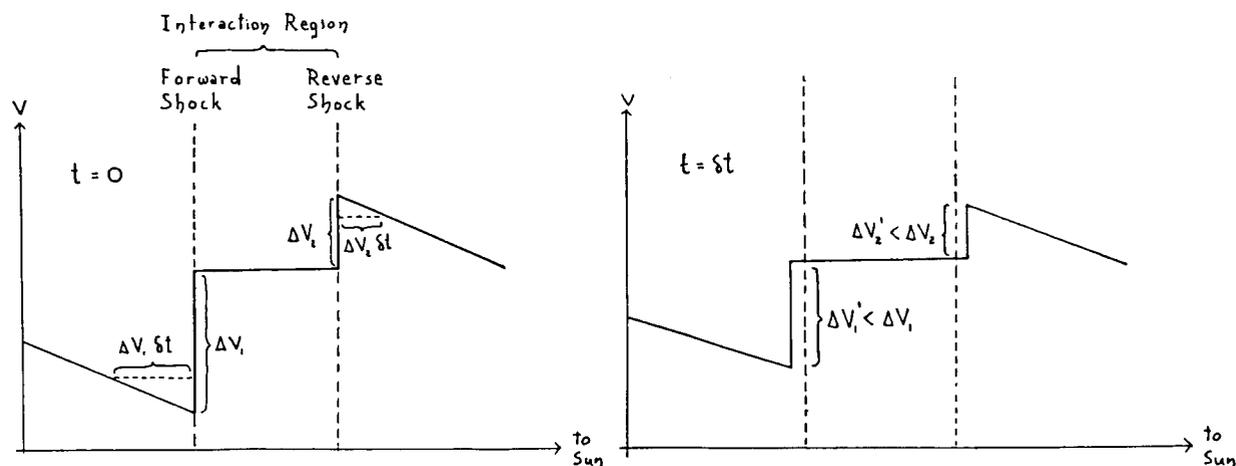
Figure 10: A schematic representation of the velocity profile across an interaction region. The top panel shows the velocity profile of an interaction region near the sun, the lower panel shows the velocity profile of the same interaction region at a larger heliocentric radius.

interaction region near to the sun, the lower panel shows the velocity profile of the same interaction region at a larger heliocentric distance. As can be seen, there are two competing processes which conspire to reduce the velocity jump across the shocks which bound the interaction regions as they are convected outward from the sun: First, the low speed material in the region which preceeds the interaction region and the high speed material in the region which follows the interaction region will be overtaken by or will overtake, respectively, the interaction region as the interaction region is convected outwards from the sun. Second, the shocks which bound the interaction region are themselves propagating into the regions outside the interaction region. But since the regions preceeding and following the interaction region contain velocity gradients, both of these effects will cause the velocity jump across the boundaries to be reduced. It is easy to see that those shocks which happen to form with a larger velocity jump will retain a larger jump than those shocks which form with a smaller velocity jump.

In summary, we observed that in our data, forward co-rotating shocks formed earlier than did the reverse co-rotating shocks: at a heliocentric distance of 2-3 AU as opposed to ≅4 AU. In many senses the forward shocks were 'stronger' than the reverse shock. The forward shocks had a larger density ratio than the reverse shocks: 3 as opposed to 2. The forward shocks were faster and had a higher velocity jump than the reverse shocks. The forward shocks were seen to occur almost twice as frequently as the reverse shocks. Finally, the forward shocks appeared to last longer than did the reverse shocks, though this observation may be due to selection effects. The reverse shocks may be becoming sufficiently weak by the end of our survey so that some of them fall below our detection threshold.

References

Axford, W. I., The interaction of the interstellar medium with the solar wind, Space Sci. Rev., 14, 582, 1973

Burlaga, L., Lepping, R., Armstrong, T., Goodrich, C., Sullivan, J., Gurnett, D., Kellogg, P., Mariani, F., Neubauer, F., Rosenbauer, H., and Schwenn, R., Interplanetary particles and fields November 22 to December 6, 1977, Helios, Voyager, and Imp observations between 0.6 and 1.6 AU, J. Geophys. Res., 85, 2227, 1980

Burlaga, L. J., Schwenn, R.,and Rosenbauer, H., Dynamical evolution of interplanetary fields and flows between 0.3 and 10 AU: entrainment, (submitted to J. Geophys. Res.), 1983

Collard, H. R., and Wolfe, J. H., Radial gradient of solar wind velocity from 1 to 5 AU, Solar Wind 3, ed. by C. T. Russel, p281, U. of California press, Los Angeles, 1974

Collard, H. R., Mihalov, J. D., and Wolfe, J. H., Radial variation of the solar wind speed between 1 and 15 AU, J. Geophys. Res., 87, 2203, 1982

Gazis, P. R., and Lazarus, A. J., Voyager observations of solar wind proton temperature: 1-10 AU, Geophys. Res. Lett., 9, 431, 1982

Goldstein, B. E., and Jokipii, J. R., Variation of solar wind parameters, J. Geophys. Res., 82, 1095, 1977

Gosling, J. T., Hundhausen, A. J., and Bame, S. J., Solar wind stream evolution at large heliocentric distances: experimental demonstration and test of a model, J. Geophys. Res., 81, 2111, 1976

Holzer, T. E., Interaction of the solar wind with the neutral component of the interstellar gas, J. Geophys. Res., 77, 5407, 1972

Holzer, T. E., Neutral hydrogen in interplanetary space, Rev. of Geophys. and Space Sci., 15, 467, 1977

Hundhausen, A. J., Nonlinear model of high-speed solar wind structure beyond 1 AU, J. Geophys. Res., 78, 1528, 1973

Kaiser, S., The far reaches of the solar wind: Pioneer 10 and Pioneer 11 plasma results, (submitted to Astrophs. J.), 1983

Pizzo, V., A three dimensional model of corotating streams in the solar wind. 3. Magnetohydrodynamic streams, J. Geophys. Res., 87, 4347, 1982

Schwenn, R., The "average" solar wind in the inner heliosphere: structure and slow variations, Solar Wind V conference, Woodstock, Vt., 1982

Siscoe, G. L., Three-dimensional aspects of interplanetary shock waves, J. Geophys. Res., 81, 6235, 1977

Smith, E. J., and Wolfe, J. H., Fields and plasmas in the outer solar system, Space Sci. Rev., 23, 217, 1979